PNNL -24681

Pacific Northwest
NATIONAL LABORATORY
Proudly Operated by Battelle Since 1965

Detection of Forced Oscillations in Power Systems with Multichannel Methods

September 2015

JD Follum

U.S. DEPARTMENT OF ENERGY

Prepared for the U.S. Department of Energy
under Contract DE-AC05-76RL01830

DISCLAIMER

PACIFIC NORTHWEST NATIONAL LABORATORY
operated by
BATTELLE
for the
UNITED STATES DEPARTMENT OF ENERGY
under Contract DE-AC05-76RL01830

Printed in the United States of America

Available to DOE and DOE contractors from the
Office of Scientific and Technical Information,
P.O. Box 62, Oak Ridge, TN 37831-0062;
ph: (865) 576-8401, fax: (865) 576-5728
email: reports@adonis.osti.gov

Available to the public from the National Technical Information Service,
U.S. Department of Commerce, 5285 Port Royal Rd., Springfield, VA 22161
ph: (800) 553-6847, fax: (703) 605-6900
email: orders@ntis.fedworld.gov
online ordering: http://www.ntis.gov/ordering.htm


This document was printed on recycled paper.
(8/00)

PNNL -24681

Detection of Forced Oscillations in Power Systems with Multichannel Methods

JD Follum

September 2015

Prepared for
the U.S. Department of Energy
under Contract DE-AC05-76RL01830

Pacific Northwest National Laboratory
Richland, Washington 99352

Summary

The increasing availability of high fidelity, geographically dispersed measurements in power systems improves the ability of researchers and engineers to study dynamic behaviors in the grid. One such behavior that is garnering increased attention is the presence of forced oscillations. Power system engineers are interested in forced oscillations because they are often symptomatic of the malfunction or misoperation of equipment. Though the resulting oscillation is not always large in amplitude, the root cause may be serious.

In this report, multi-channel forced oscillation detection methods are developed. These methods leverage previously developed detection approaches based on the periodogram and spectral-coherence. Making use of geographically distributed channels of data is shown to improved detection performance and shorten the delay before an oscillation can be detected in the online environment. Results from simulated and measured power system data are presented.

Acknowledgments

I would like to acknowledge Bonneville Power Administration for providing financial support and data needed to complete this research. I would also like to thank Dr. Ning Zhou of Binghamton University and Dr. Frank Tuffner of Pacific Northwest National Lab for providing their insights on the research topic.

Acronyms and Abbreviations

CDF	Cumulative Distribution Function
CG	Coherent Gain
DC	Direct Current
GMSC	Generalized Magnitude Squared Coherence
GLRT	Generalized Likelihood Ratio Test
kV	Kilovolt
MSC	Magnitude Squared Coherence
OSNR	Output Signal-to-Noise Ratio
P_D	Probability of Detection
P_{FA}	Probability of False Alarm
PMU	Phasor Measurement Unit
PSD	Power Spectral Density
WECC	Western Electricity Coordinating Council

Contents

Figures

Tables

1.0 Introduction

In recent years, forced oscillations have become a topic of renewed interest to power system operators. This renewed interest is due in large part to the installation of extensive phasor measurement unit (PMU) networks that provide high-fidelity, time-synchronized measurements from across the large geographical areas that power systems span. Analysis of PMU data has revealed that forced oscillations appear in power systems with surprising regularity. Though not a threat to the grid's stability, forced oscillations are often indicative of equipment malfunction or improper operation. Thus, system operators are interested in knowing when forced oscillations are occurring so that the root problem can be identified and addressed.

Identifying when forced oscillations are present is challenging because they appear in PMU data with a wide range of amplitudes and are not always apparent above ambient noise in time-domain data. Considering the large number of PMUs that a system may contain, visual inspection is impractical, even in cases where the oscillation amplitude is large. Thus, automated methods of detecting forced oscillations are necessary.

Forced oscillation detection algorithms were proposed in [Follum, 2015], [Zhou, 2013], and [Zhou, 2014]. All three methods rely on spectral analysis of signals from a single PMU. One of the advantages of PMU data is that it is time synchronized across geographical areas. By simultaneously analyzing data from multiple PMUs, the performance of detection algorithms can be improved. Increased reliability in detecting small oscillations and faster detection of large oscillations can be expected from successful multichannel algorithms.

In this project, the previously mentioned single channel algorithms were expanded to multiple channels. The initial algorithms and their subsequent extensions are described in Sections 2 and 3, respectively. Results from experiments with simulated and measured power system data are presented in Section 4. Concluding remarks and expectations for future work are provided in Section 5.

2.0 Detection Algorithms

In this section, multi-channel extensions to the algorithms proposed in [Follum, 2015] and [Zhou, 2014] will be discussed. For both algorithms, the extensions are achieved by combining the test statistics from individual channels. A test statistic is a value that is checked against a threshold to determine the outcome of a test. In this case, when a test statistic exceeds the threshold, a forced oscillation is detected. For any test, the choice of the threshold plays a fundamental role in the test's performance. If the threshold is too low, many false alarms[1] will occur. If the threshold is too high, many forced oscillations will go undetected. Discussion on setting a proper threshold will be provided for each of the algorithms. The multi-channel extensions of the periodogram method described in [Follum, 2015] and the spectral-coherence method described in [Zhou, 2014] will be described in Sections 2.1 and 2.2, respectively.

[1] Throughout this report the term *alarm* is used in a statistical sense and does not indicate that the user should necessarily be notified. Practical detector implementations require higher-level logic to determine what information is passed to the user in the event of an alarm.

2.1 The Periodogram Method

As its namesake implies, the periodogram method operates by comparing a combination of periodograms to a threshold. Periodograms are simple measures of a signal's power as it varies with frequency. If the periodogram is unusually high at a particular frequency, it indicates that an oscillation is present in the signal at that frequency. Using the statistical distributions of the multiple periodograms, the threshold for the method is established with relation to probabilities of detection and false alarm. As described in this report, the threshold must be adjusted to account for the correlation between measurements from different channels. For reference throughout this section, an illustration of the method's operation is provided in Figure 1.

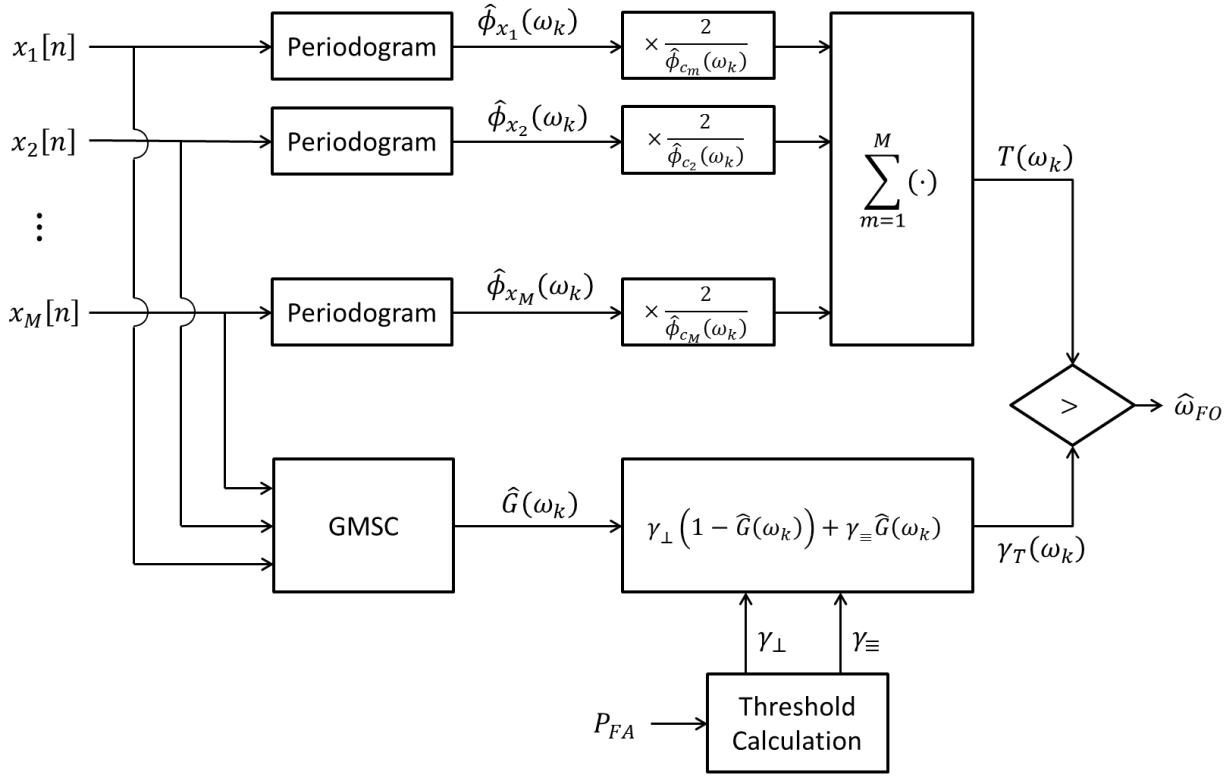

Figure 1: Flowchart for the multi-channel periodogram-based detector.

Because periodograms measure signal power as a function of frequency, one of the challenges in applying this approach for power systems is that the power of ambient measurements varies with frequency. If this characteristic is not addressed, the detector will perform poorly. This concept is illustrated in Figure 2. At frequencies where the signal power is high, the periodogram will often exceed the threshold, even when a forced oscillation is not present. Where it is low, the forced oscillation must be very large to cross the threshold. This challenge was addressed in detail for a single channel in [Follum, 2015]. An approach to address the challenge with a multi-channel version of the periodogram algorithm can be motivated by first considering a simplified case.

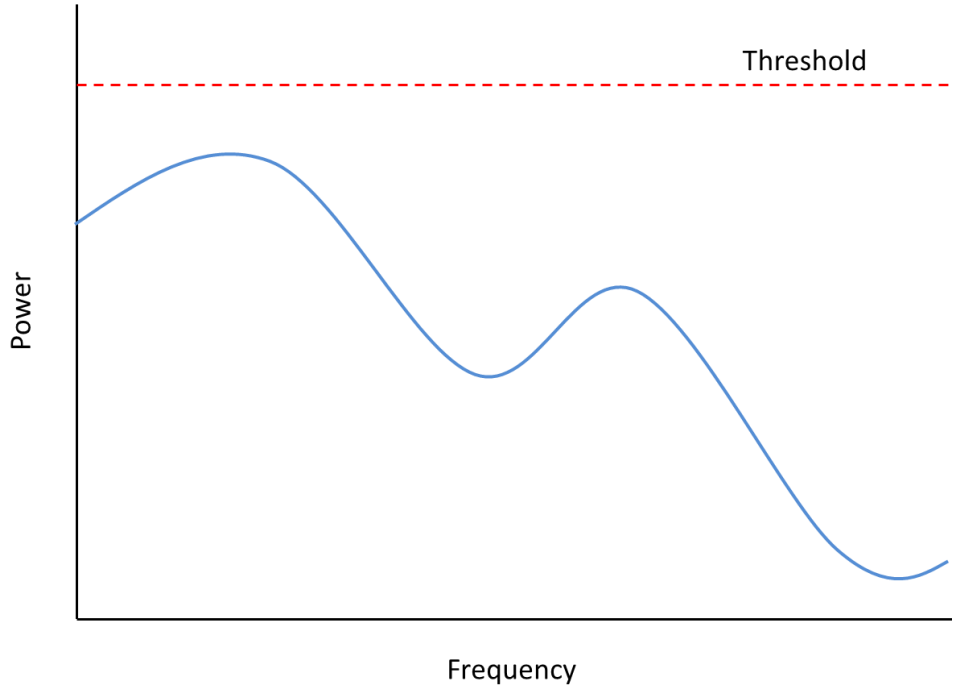

Figure 2: Illustration of an ambient noise spectrum and a detection threshold.

In Section 13.6.6 of [Kay, 1998], the detection of a deterministic signal with unknown parameters in circular white Gaussian noise is considered. As shown in Appendix A, in the special case where the noise is real and the signal of interest is a sinusoid with unknown amplitude, phase, and frequency, the test statistic for the Generalized Likelihood Ratio Test (GLRT) is

$$T_w(\omega_k) = \sum_{m=1}^{M} \frac{2\hat{\phi}_{x_m}(\omega_k)}{\sigma^2} \tag{1}$$

where

$$\omega_k = \frac{2\pi k}{N^{(0)}}, \qquad 0 \le k \le \frac{N^{(0)}}{2}$$

is the frequency variable with units of radians per sample, σ^2 is the variance of the white noise, and

$$\hat{\phi}_{x_m}(\omega_k) = \frac{1}{NU}\left|\sum_{n=0}^{N-1} x_m[n]v[n]e^{-j\omega_k n}\right|^2$$

is the periodogram of x_m, the m^{th} channel of data containing N samples. The periodogram is zero padded to length $N^{(0)}$ and is calculated with a window $v[n]$ with associated scaling parameter

$$U = \frac{1}{N}\sum_{n=0}^{N-1} v^2[n]$$

Thus, the test operates by comparing the scaled sum of periodograms from each channel to a threshold. Forced oscillations are detected at frequencies where the test statistic exceeds the threshold. These frequencies are denoted as $\widehat{\omega}_{FO}$ in Figure 1 for the practical implementation of the method, which will now be described.

Adaptation of the test statistic in (1) for use with the colored ambient noise of power systems is straight forward. In (1), the frequency-invariant power of the ambient noise is accounted for with the term σ^2. The analogous parameter for colored noise is the Power Spectral Density (PSD). The PSD is the theoretical power of the noise as it varies with frequency and is given by

$$\phi_{c_m}(\omega) = \lim_{N\to\infty} E\left\{\frac{1}{N}\left|\sum_{n=0}^{N-1} c_m[n]e^{-j\omega n}\right|^2\right\}$$

where $c_m[n]$ denotes the ambient noise component of the measured signal at channel m. Using the PSD, the test statistic for the multi-channel periodogram-based detector follows from (1) as

$$T(\omega_k) = \sum_{m=1}^{M} \frac{2\hat{\phi}_{x_m}(\omega_k)}{\phi_{c_m}(\omega_k)} \tag{2}$$

The PSD is a theoretical term, so for practical implementation of the detector it must be replaced with an estimate, a topic that will be discussed later in the report. Its use here leads to expressions for detection thresholds with associated probabilities of false alarm (P_{FA}), the probability that the test statistic will exceed the threshold even though an oscillation is not present. In detection problems, this parameter is often selected by the user. Another parameter of interest, the probability of detection (P_D) is the probability that an oscillation with given parameters, e.g., amplitude, will cause the test statistic to exceed the threshold and be detected. There is an intuitive tradeoff between P_{FA} and P_D, with improved detection performance being achieved at the cost of more false alarms. Because of this tradeoff, these probabilities are fundamental in characterizing the performance of a detector.

As shown in [Follum, 2015], theoretical expressions relating the detection threshold to P_{FA} and P_D can be obtained for the single-channel periodogram method. For the multi-channel extension, such expressions do not exist, though an alternative method of relating the threshold to P_{FA} will be described shortly. An expression for P_D, though, is not possible to obtain with the following method.

To relate the detection threshold to P_{FA} and P_D, the statistical distribution of the test statistic is needed. A challenge in obtaining this distribution arises in that the channels of data are not independent. To address this challenge, the distribution is derived for two cases: all channels independent and all channels identical. The results are then combined to account for the true relationship between the channels, which lies between independent and identical.

The case where all channels are independent is considered in Appendix B. The resulting threshold that corresponds to a maximum theoretical P_{FA} is

$$\gamma_{\perp} = F_{\chi^2_{2M}}^{-1}\left(1 - \frac{P_{FA}^{max}}{B}\right)$$

where $F_{\chi'^2_d(\lambda)}^{-1}(\cdot)$ denotes the inverse Cumulative Distribution Function (CDF) of the chi-squared random variable with d degrees of freedom and B denotes the number of frequency bins, i.e., ω_k, that are examined. Functions for the calculation of the inverse CDF are readily available in multiple software packages. The other extreme, where all channels are identical, is considered in Appendix C. The threshold for this case is

$$\gamma_{\equiv} = M \times F_{\chi^2_2}^{-1}\left(1 - \frac{P_{FA}^{max}}{B}\right)$$

In practice, the threshold that will achieve the specified P_{FA}^{max} will be located between $\gamma_{\perp}$ and $\gamma_{\equiv}$, with values depending on the relationship between the channels. Though there is likely no theoretical way to express this threshold, an intuitive approach based on the Generalized Magnitude Squared Coherence (GMSC) described in [Ramirez, 2008] has been developed. The GMSC, which is formulated mathematically in Appendix D, reflects how linearly correlated multiple time series are as a function of frequency. The GMSC takes on values between zero and one, with values near one indicating a linear relationship between the channels. With these characteristics, the GMSC can serve as an intuitive basis for setting the threshold between $\gamma_{\perp}$ and $\gamma_{\equiv}$. At frequencies where the GMSC is near zero, the channels are nearly independent and the threshold should be near $\gamma_{\perp}$. When the GMSC is near one, the channels are highly related and the threshold should be near $\gamma_{\equiv}$. Following this approach, the threshold is given by

$$\gamma_T(\omega) = \gamma_{\perp}\left(1 - \hat{G}(\omega)\right) + \gamma_{\equiv}\hat{G}(\omega) \tag{4}$$

where $\hat{G}(\omega)$ denotes the GMSC estimate. Note that the dependence of $\gamma_T(\omega)$ on the GMSC necessitates that the threshold is also be a function of frequency. A theoretical association between this threshold and the specified P_{FA}^{max} does not exist, but the empirical results presented in Section 3 demonstrate that its use allows the method to approach desired performance much closer than the use of either $\gamma_{\perp}$ or $\gamma_{\equiv}$.

To implement the detector practically, the PSD used in the test statistic given by (2) and the GMSC used to set the threshold in (4) must be estimated. There are multiple ways that these values could be estimated, each with their own ramifications. The results in this report were generated by estimating the PSD and GMSC in an online fashion, meaning that the same measurements tested for the presence of forced oscillations were used to estimate the PSD and GMSC. This counterintuitive approach was made possible by the implementation of a novel spectral estimation technique.

The difficulty in estimating the PSD and GMSC in the online environment is that forced oscillations present in the measurement data cause sharp peaks in the spectral estimates at the frequencies of the oscillations. If the peaks in the PSD estimate are unaccounted for, they remove the corresponding peaks in the test statistic needed for the forced oscillation to be detected. Peaks in the GMSC lead to an unnecessarily high threshold at the frequency of the forced oscillation that severely impairs detection performance. To address this issue, a median filter is applied to estimates of the PSD and GMSC calculated with Welch's method of averaging. Median filters tend to remove narrow peaks in the signal

they are applied to, making them ideal for this application. Welch's method of spectral estimation relies on partitioning the signal into overlapping windows and averaging periodograms from each window. To achieve necessarily narrow peaks at forced oscillation frequencies, the amount of averaging in the Welch estimates must be limited. The median filter also helps to smooth the estimates, which tend to be highly variable due to the limited averaging. Thus, the approach used here is a combination of Welch's method and an adapted version of the Daniell method, which produces spectral estimates by applying conventional filters to simple periodograms [Stoica, 2005].

The use of PSD and GMSC estimates, especially ones generated in the online environment, along with the need to scale the detection threshold based on the correlation of the signals, causes the detector's performance to vary from theoretical values. The theoretical foundation of the method is still very valuable in guiding the setup of the detector for practical use. It may also be possible to use PSD and GMSC estimates calculated offline. This approach avoids the difficulty of removing the influence of forced oscillations, but removes the detector's ability to adapt to changing system conditions. Such an approach would also require periodic updates of the PSD and GMSC estimates, which requires significant expertise. Multiple approaches to estimating the PSD and GMSC exist, and each likely offers advantages and disadvantages for specific applications. The scope of this research focused on operation in the online environment, leading to the approach just described.

2.2 The Spectral Coherence Method

The premise of spectral coherence methods is that signals containing the same forced oscillation will demonstrate high spectral coherence at the frequency of the oscillation. The spectral coherence of two separate channels of data was examined in [Zhou, 2013]. This method does not account for spectral coherence that exists between different channels of power system measurements due to the system's dynamics. This natural coherence can be difficult to distinguish from coherence arising due to forced oscillations. This issue is addressed in the self-coherence method proposed in [Zhou, 2014] by considering the spectral coherence between a signal and the time-delayed version of the signal. Without the delay, the self-coherence would be identical to one, the highest possible value of the coherence spectrum, at all frequencies. If the underlying ambient noise was white, a delay of a single sample would be sufficient to ensure independence of the two signals. Because the ambient noise of power systems is colored by the system's dynamics, longer delays are necessary. Incorporating a sufficient delay significantly reduces the coherence between signals and allows the algorithm to detect persistent forced oscillations, which remain correlated regardless of delay.

The method reported here is an extension of the self-coherence method to multiple delays and multiple channels. The algorithm's operation is illustrated in Figures 3 and 4. Figure 3 demonstrates the portion of the algorithm that operates on an individual channel's measurements. The input signal is first delayed D times by Δn samples. An estimate of the GMSC between the resulting $D + 1$ signals termed the self-GMSC is then calculated. The GMSC is a multi-channel extension of the spectral coherence with values near zero indicating low coherence and values near one indicating high coherence [Ramirez, 2008]. The GMSC is described in greater detail in Appendix D. Incorporating multiple delays reduces the correlation between the ambient noise components of the measurements, while further highlighting the coherence of the forced oscillation components.

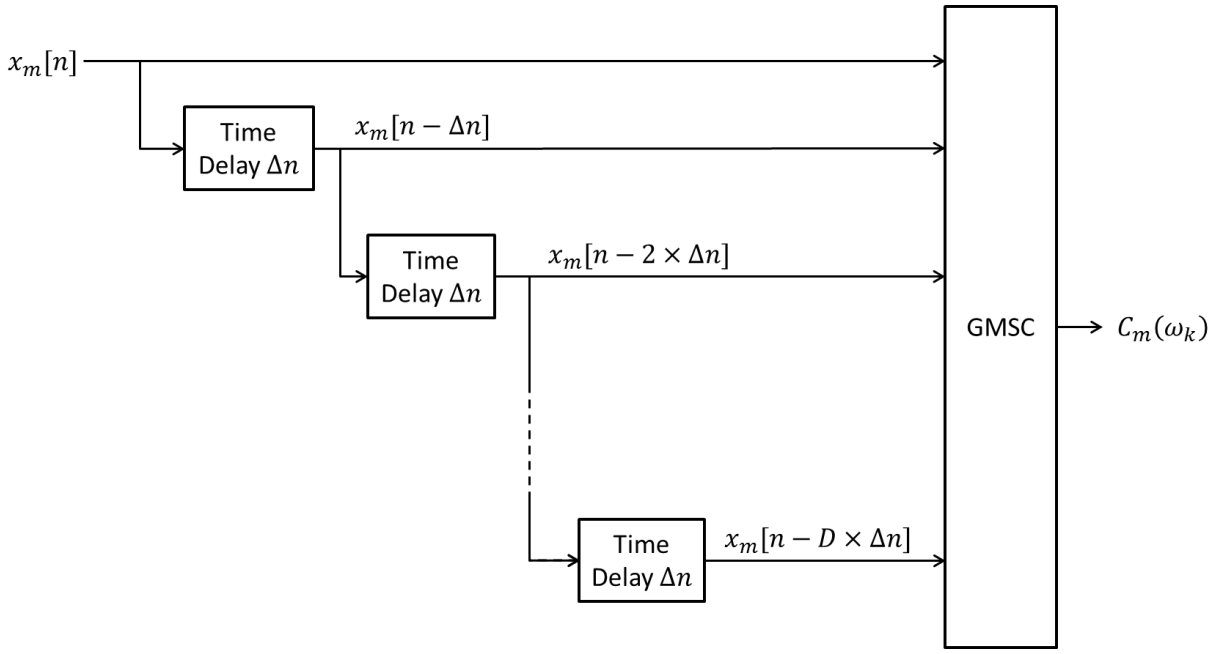

Figure 3: Flowchart describing the calculation of the self-GMSC for a single channel.

After the self-GMSCs are calculated for each channel, they are averaged together, as illustrated in Figure 4. This averaging reduces the variation in the spectrum's noise floor due to the noise's stochastic nature, making peaks due to forced oscillations more apparent. The output of this averaging serves as the test statistic for the multi-channel spectral coherence method. Forced oscillations are detected at frequencies where the test statistic, $C(\omega_k)$, exceeds a threshold.

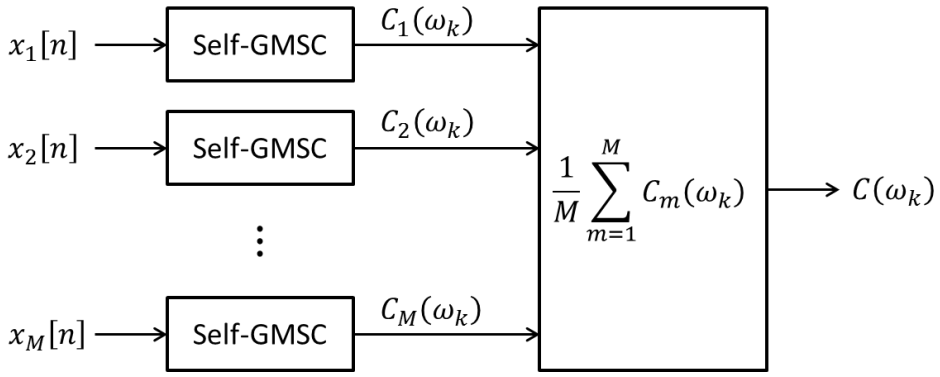

Figure 4: Flowchart describing the calculation of the spectral coherence method's test statistic.

An expression for a threshold related to probabilities of detection and false alarm is not available for the spectral coherence method. However, the introduction of delays in the self-GMSC portion of the algorithm establishes a relatively flat noise floor in the test statistic, so a frequency-dependent threshold is not required, as it is for the periodogram method. Several methods for choosing a threshold exist. Because the test statistic is limited to the range between 0 and 1, an intuitive threshold such as 0.7 can be set, but offers no adaptation for different system conditions, number of channels, etc. A more advanced approach could be bootstrapping using measurement based system models, but this approach could be quite

complex and difficult to parameterize properly. In this report, the threshold is set based on the median of the test statistic across all considered frequency bins. The median is robust against large outlying values at forced oscillation frequencies, so it serves as a measure of the noise floor level. The threshold is given by

$$\gamma_c = c \times \underset{\omega_k \in \Omega_B}{\text{med}} [C(\omega_k)]$$

where the test statistic is

$$C(\omega_k) = \frac{1}{M} \sum_{m=1}^{M} C_m(\omega_k)$$

and $C_m(\omega_k)$ denotes the self-GMSC spectrum for the m^{th} channel. The scalar c provides control over the tradeoff between the algorithm's ability to detect oscillations and the frequency of false alarms.

3.0 Experimental Results

After the methods described in this report were developed, experiments were conducted to compare their performance and establish best practices for their use. Experiments were conducted with simulated power system data to examine the statistical performance of the methods. Analysis of measured PMU data provided insight into their performance in real-world conditions.

3.1 Results from Simulated Data

Simulated data was generated using a simplified model of the Western Electricity Coordinating Council (WECC) system known as the miniWECC. A detailed description of the miniWECC is contained in [Trudnowski, 2013] and the references therein. Here, a brief overview is provided. To obtain the model, generation for many areas is grouped into an equivalent machine and only transmission lines with significant length and a rating of at least 230-kV are included. The model contains 34 generators, 115 lines and high-voltage transformers, 54 generator and load transformers, 19 load buses, and 2 DC lines.

To generate data, the model is linearized about an operating point and represented in state-space form. A small portion of each load is modeled as random. This random perturbation excites the system's modes. Forced oscillations can be modeled by adding square wave inputs at a generator bus to reflect the generator entering a stable limit cycle. This approach requires that new data is generated for each forced oscillation frequency and amplitude under consideration. For the tests reported here, many frequencies and amplitudes were considered, making this modeling approach infeasible. Instead, the model was used to generate a base set of ambient data. By analyzing the linear model for a given oscillation fundamental frequency, the amplitudes and phases of the oscillation's harmonics at each output were calculated. With this information, the forced oscillations were added to the existing ambient data. The two modeling methods were verified to produce identical outputs.

Using the model, 1000 trials of ambient data were generated. The use of many statistically independent trials to analyze a methods performance is known as Monte Carlo analysis. Each trial was 10 minutes in duration. The full 10 minutes was analyzed by the periodogram method, which requires a

relatively large set of data to estimate the noise spectrum and GMSC with sufficiently low variance. The spectral-coherence method, however, was implemented with a delay of 10 seconds between 1 minute long analysis windows. If larger analysis windows were used, the delay between them would need to increase accordingly to ensure small coherence. The increased delay between analysis windows would in turn lead to longer detection delays in the online environment. As will be seen in the following sections, the amount of analyzed data plays a role in detection performance.

3.1.1 Results for the Periodogram Method

The first test of the periodogram method was designed to verify that use of the detection threshold given by (4) results in the expected number of false alarms. To do this, 1000 sets of ambient data were examined. The test statistic in (2) was calculated for each of the 10 minute datasets. Based on these test statistics, the threshold $\hat{\gamma}_T(\omega_k)$ was selected such that 50 false alarms occurred at frequency bin. Note that this does not indicate an overall P_{FA} of 0.05 because each bin was considered individually. Theoretical thresholds $\gamma_\perp$ and $\gamma_\equiv$ were calculated to achieve the same number of false alarms. With these thresholds, $\gamma_T(\omega_k)$ was calculated using the true GMSC. Plots comparing these thresholds are presented in Figures 5 and 6 for four channels and eight channels, respectively. Note that in both cases, the scaled threshold $\gamma_T(f)$, with the f denoting units of Hz, better matches the empirical threshold $\hat{\gamma}_T(f)$ than either $\gamma_\perp$ or $\gamma_\equiv$. Though the scaling of $\gamma_T(f)$ is based on reasoning rather than strict theory, there is clearly a relationship between $\gamma_T(f)$ and $\hat{\gamma}_T(f)$ that lends credibility to the way it is calculated.

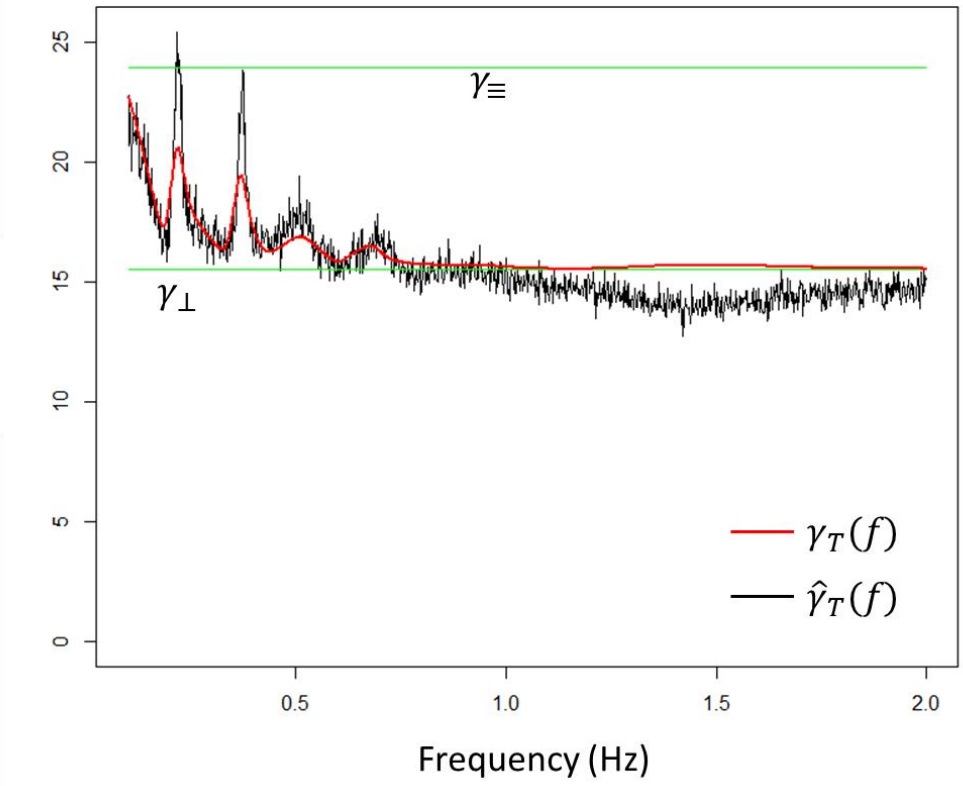

Figure 5: Comparison of theoretical – $\gamma_T(f)$ – and empirical – $\hat{\gamma}_T(f)$ – thresholds for four channels.

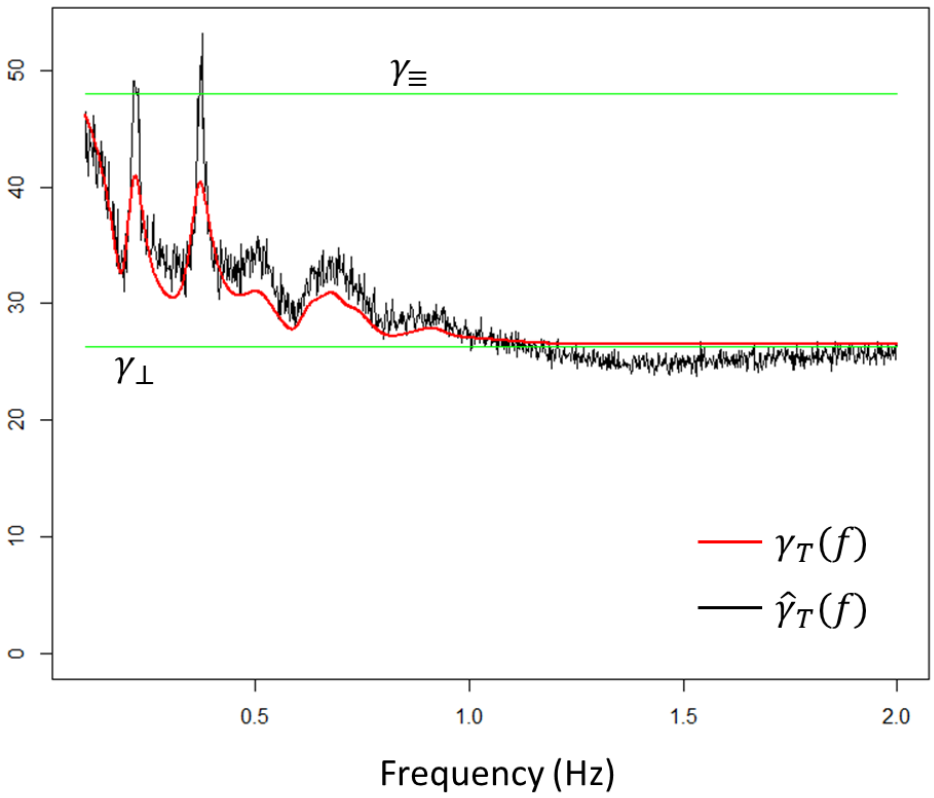

Figure 6: Comparison of theoretical – $\gamma_T(f)$ – and empirical – $\hat{\gamma}_T(f)$ – thresholds for eight channels.

The next test for the multi-channel periodogram method focused on the probability of false alarm. The 1000 trials of ambient data were again examined with a desired P_{FA} of 0.05. Estimates of the GMSC between channels were used to scale the detection threshold between $\gamma_{\perp}$ and $\gamma_{\equiv}$. As can be seen in Table 1, the thresholds that assume the channels are independent or identical perform poorly. The low P_{FA} observed for $\gamma_{\equiv}$ may seem desirable, but it indicates that the threshold will provide poorer detection performance than the scaled threshold. The observed probabilities of false alarm for the scaled threshold are closest to the specified value, indicating that the scaling approach to setting the threshold is reasonable.

Table 1. Observed probabilities of false alarm for various detection thresholds

M	P_{FA}	Observed P_{FA} for $\gamma_{\perp}$	Observed P_{FA} for $\gamma_{\equiv}$	Observed P_{FA} for $\gamma_T(\omega_k)$
4	0.05	0.411	0.001	0.011
8	0.05	0.991	0.001	0.031

After formulating the detection threshold and demonstrating that it provided acceptable performance in regard to false alarms, the algorithm was tested to determine the value of analyzing multiple signals. These tests consisted of applying the algorithm to 1000 trials of data containing a forced oscillation at 0.35 Hz. Each trial contained 10 minutes of data, and a P_{FA} of 0.001 was used.

In the first test, the algorithm was applied to datasets containing from one to eight channels. Several forced oscillation amplitudes were considered as well. These amplitudes are expressed in terms of the ratio between the amplitude and twice the value of the noise spectrum at the oscillation's frequency. This ratio was shown to be a primary factor in determining the algorithm's detection performance in [Follum, 2015] and can be viewed similarly to the more familiar signal-to-noise ratio. Observed detection performance over the 1000 trials is plotted in Figure 7. Because the ratio specifying oscillation amplitude varies from channel to channel, the maximum over all eight channels was used to form the x-axis. Note that the use of multiple channels improves detection performance considerably.

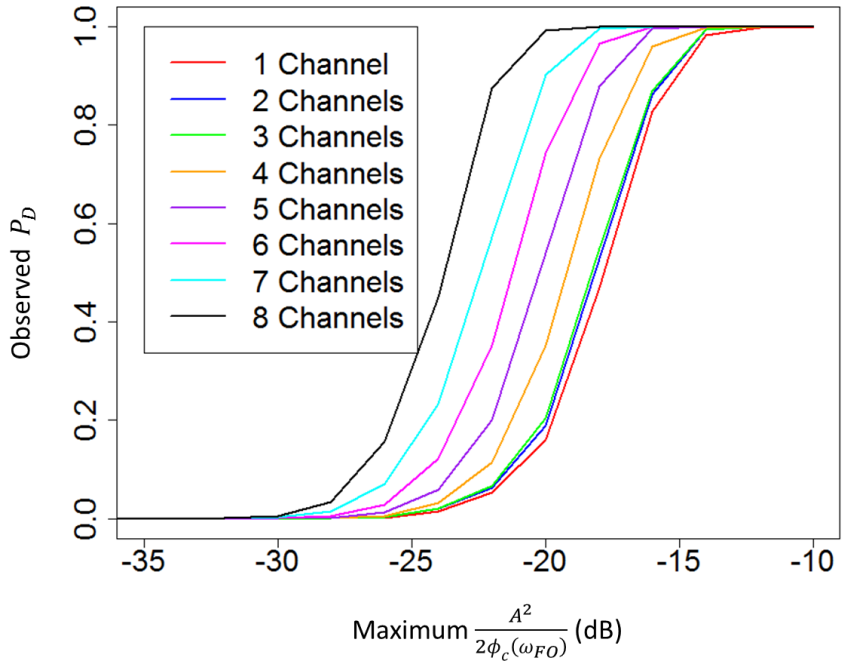

Figure 7: Detection performance of the periodogram method for various numbers of channels and forced oscillation amplitudes.

A metric of practical importance for forced oscillation detection is the time required to detect oscillations in the online environment. Recall that the methods proposed in this report rely on past data to operate. When an oscillation begins in the system, it is desirable to detect it quickly. As demonstrated in Figure 8, the detection performance of the method increases with the duration of the oscillation within the ten-minute analysis window and the number of examined channels. To generate this plot, an oscillation with $\frac{A^2}{2\phi_c(\omega_{FO})}$ equal to -10 dB was used. In this case, the oscillation can be reliably detected using eight channels over a minute earlier than when a single channel is examined. For some applications, this difference in detection time may be significant. Detection performance as a function of oscillation duration was also examined for $\frac{A^2}{2\phi_c(\omega_{FO})}$ equal to 0 dB, and results are presented in Figure 9. The large

oscillation amplitude largely removes the advantage of using multiple channels, but these results are valuable for comparison with the spectral-coherence method in the next section.

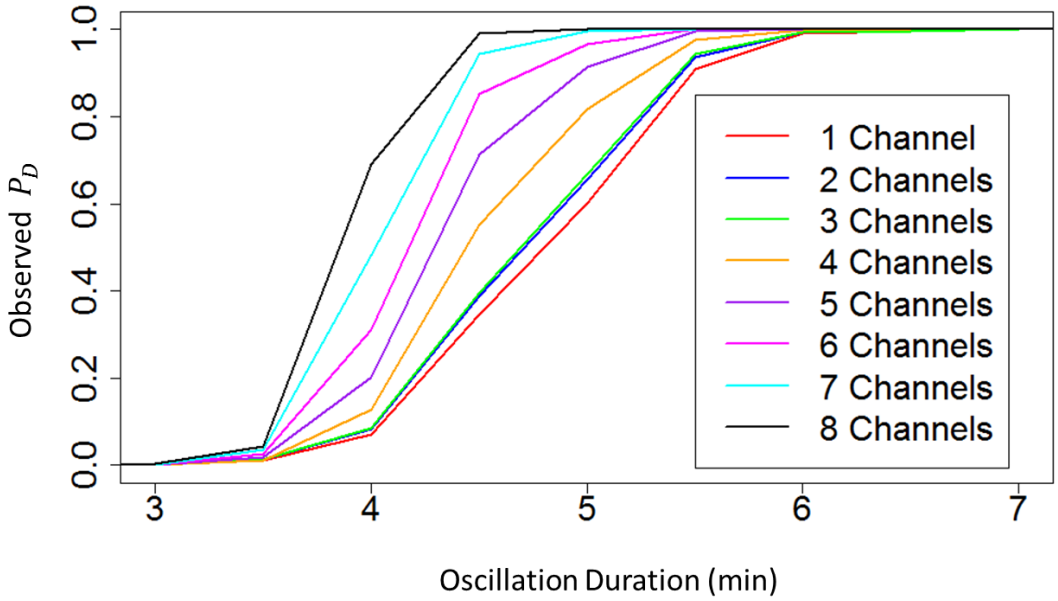

Figure 8: Detection performance of the periodogram method for various numbers of channels and forced oscillation durations with $\frac{A^2}{2\phi_c(\omega_{FO})} = -10\ dB$.

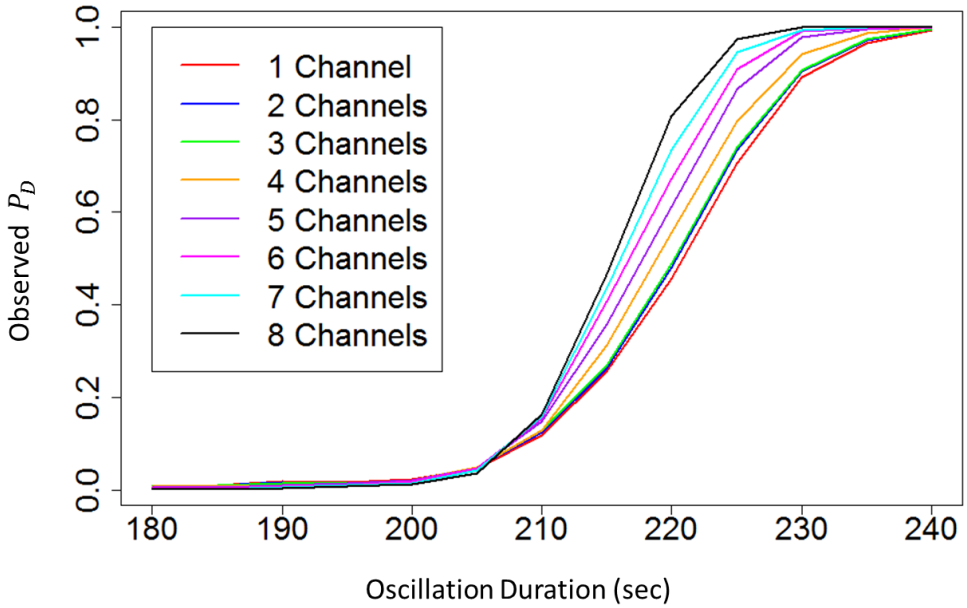

Figure 9: Detection performance of the periodogram method for various numbers of channels and forced oscillation durations with $\frac{A^2}{2\phi_c(\omega_{FO})} = 0\ dB$.

3.1.2 Results for the Spectral-Coherence Method

The spectral-coherence method was tested in much the same way and with the same dataset as for the periodogram method. With no theoretical basis for setting the P_{FA}, the first test was conducted to set threshold scaling parameters for later tests of the method's detection performance. Recall that for the spectral-coherence method, the threshold is set by scaling the median of the test statistic by a scalar c. Table 2 lists the threshold scaling parameters needed for a single false alarm out of the 1000 examined trials. Note that the scaling parameter tends to decrease as the number of channels increases, particularly for the first four channels. These numbers will vary for the considered channels and should not be considered general results applicable to any system. They were, however, useful in testing the method's detection performance.

Table 2. Threshold scaling parameters required to achieve a single false alarm out of 1000 trials for various numbers of channels.

Number of Channels *M*	**Threshold Scaling Parameter c**
1	9.76
2	6.52
3	6.90
4	5.64
5	5.64
6	5.88
7	5.61
8	5.58

To test the method's ability to detect forced oscillations, the algorithm was applied to simulated datasets with the threshold scaling parameters listed in Table 2. Observed detection performance over the 1000 trials is plotted in Figure 10. The considered forced oscillation amplitudes are again expressed in terms of the ratio between the amplitude and twice the value of the noise spectrum at the oscillation's frequency. Note that the use of multiple channels improves detection performance considerably. In comparing Figures 7 and 10, it is clear that the periodogram method can reliably detect much smaller forced oscillations. Recall, though, that the spectral-coherence method operates on significantly less data.

The self-coherence method's suitability to operation on less data is a disadvantage for detecting forced oscillations with small amplitudes, but it is advantageous for the fast detection of large-amplitude

oscillations in the online environment. To test the method's detection delay, it was applied 1000 trials of simulation data containing forced oscillations with durations ranging from 10 to 80 seconds. Amplitudes were set such that the maximum $\frac{A^2}{2\phi_c(\omega_{FO})}$ over all channels was equal to 0 dB. Results are presented in Figure 11. Note that the addition of multiple channels dramatically reduces the amount of time required to reliably detect the forced oscillation.

It is interesting to compare the corresponding results from the periodogram method in Figure 9. Note that the forced oscillation must persist for multiple minutes before the periodogram method is able to reliably detect it. Though the periodogram method offers better detection of small oscillations, the spectral-coherence method is able to detect large oscillations faster in the online environment. These results point to the complementary nature of the methods.

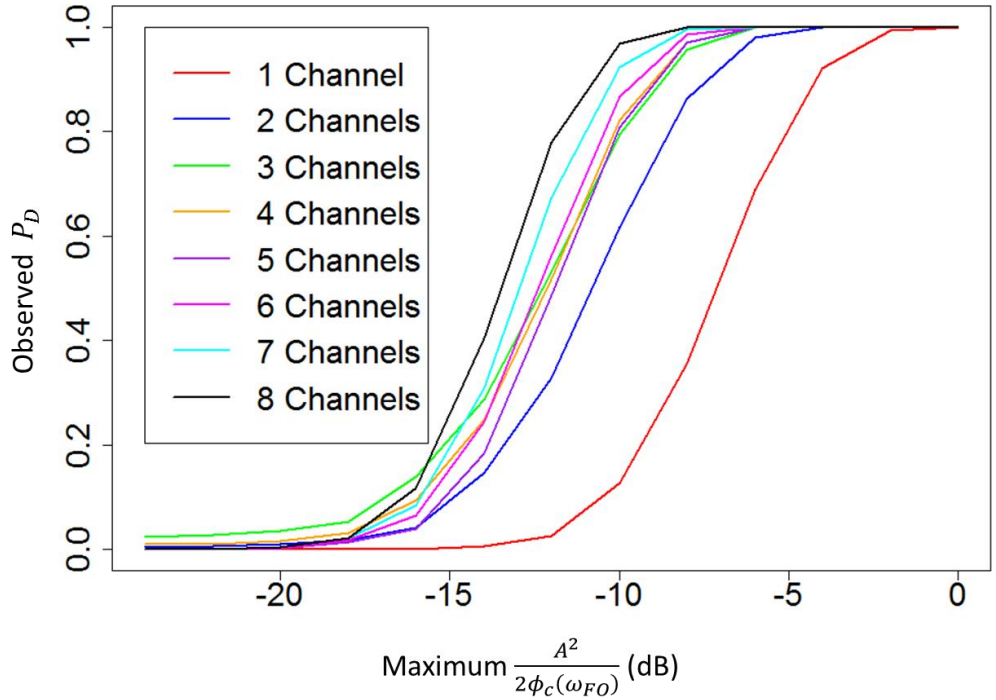

Figure 10: Detection performance of the spectral-coherence method for various numbers of channels and forced oscillation amplitudes.

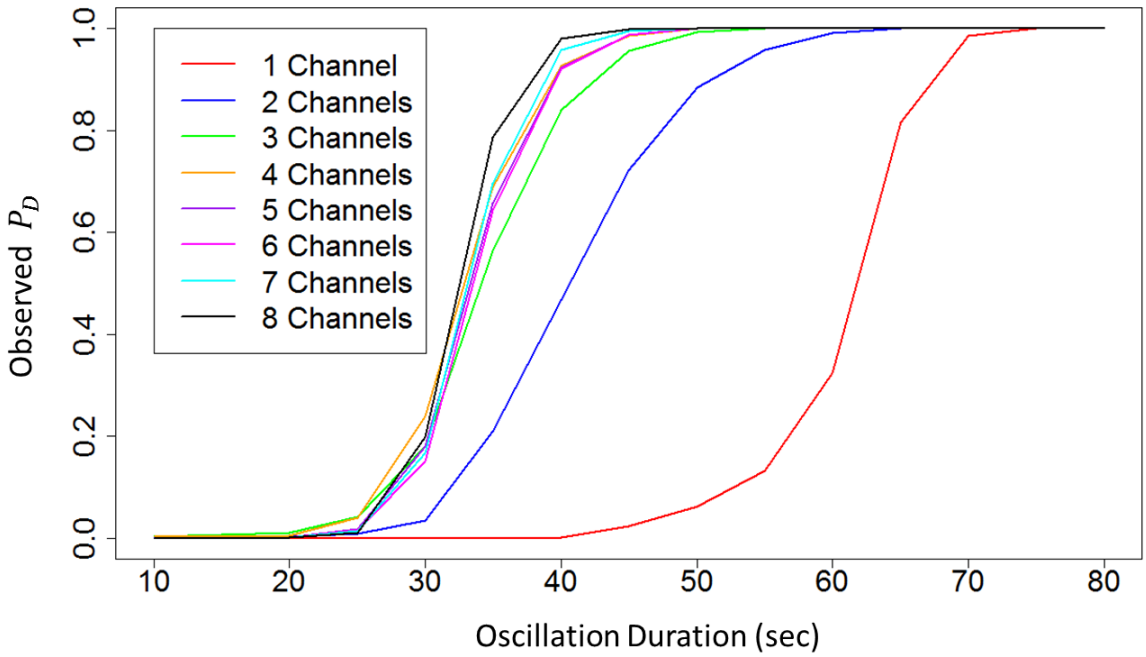

Figure 11: Detection performance of the spectral-coherence method for various numbers of channels and forced oscillation durations with $\frac{A^2}{2\phi_c(\omega_{FO})} = 0\ dB$.

3.2 Results from Measured Data

After testing the performance of the methods with simulation data, they were applied to measured PMU data to verify that they can be successfully applied in practical applications. The methods were implemented in much the same way as for the simulated data. They were applied to two hours of data collected from six channels of data spread throughout the WECC system. Further details on the data are omitted to protect the confidentiality of the data.

Results for the periodogram method are presented in Figure 12 and those for the spectral-coherence method are presented in Figure 13. Note that forced oscillations were present for the entirety of the two hour dataset. Further examination of the dataset revealed that all oscillations were too small to be visible in the time-domain data. To focus on larger oscillations and/or reduce the occurrence of false alarms, the P_{FA} (periodogram method) and threshold scaling parameter (spectral-coherence method) could be increased. However, even oscillations with small amplitudes can indicate misoperation of equipment, so the ability of the methods to detect these small oscillations is valuable.

From Figures 12 and 13, it is clear that the methods detect several of the same oscillations. The periodogram method, being better suited to low-amplitude oscillations, detects oscillations at frequencies that the spectral-coherence method misses. The periodogram method also offers higher frequency resolution of the forced oscillation frequencies due to its longer analysis window. With its shorter analysis windows, the spectral-coherence method appears to detect the low-frequency oscillation beginning between minutes 40 and 60 faster. Thus, the strengths and weaknesses of each method are demonstrated with these measurement results.

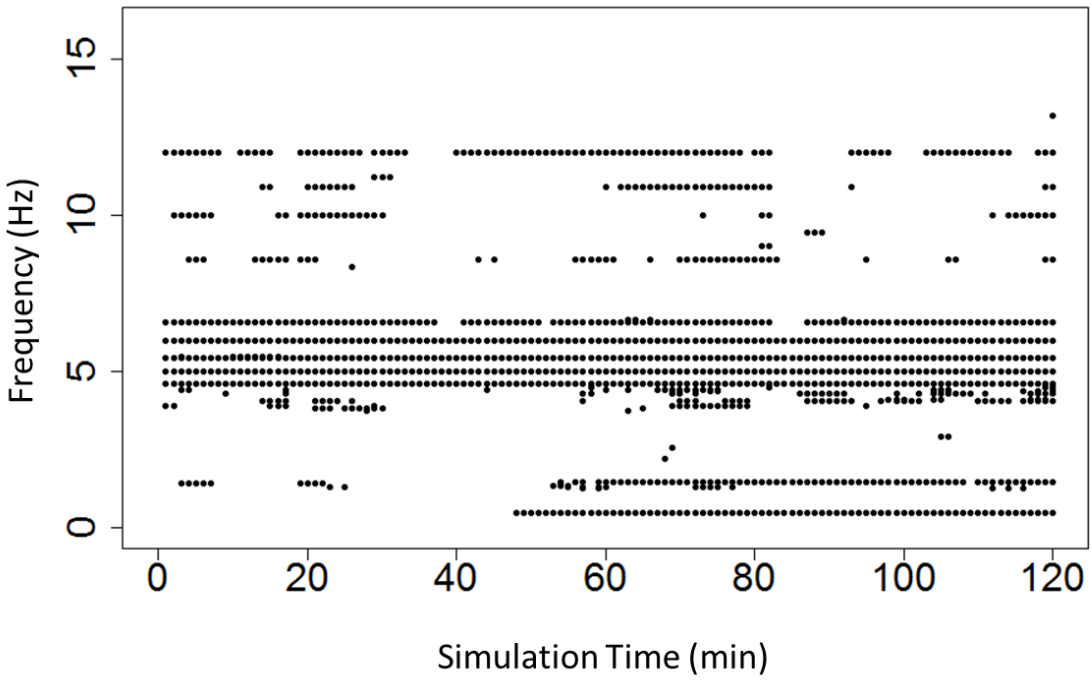

Figure 12: Detected forced oscillations in two hours of measurement data using the periodogram method.

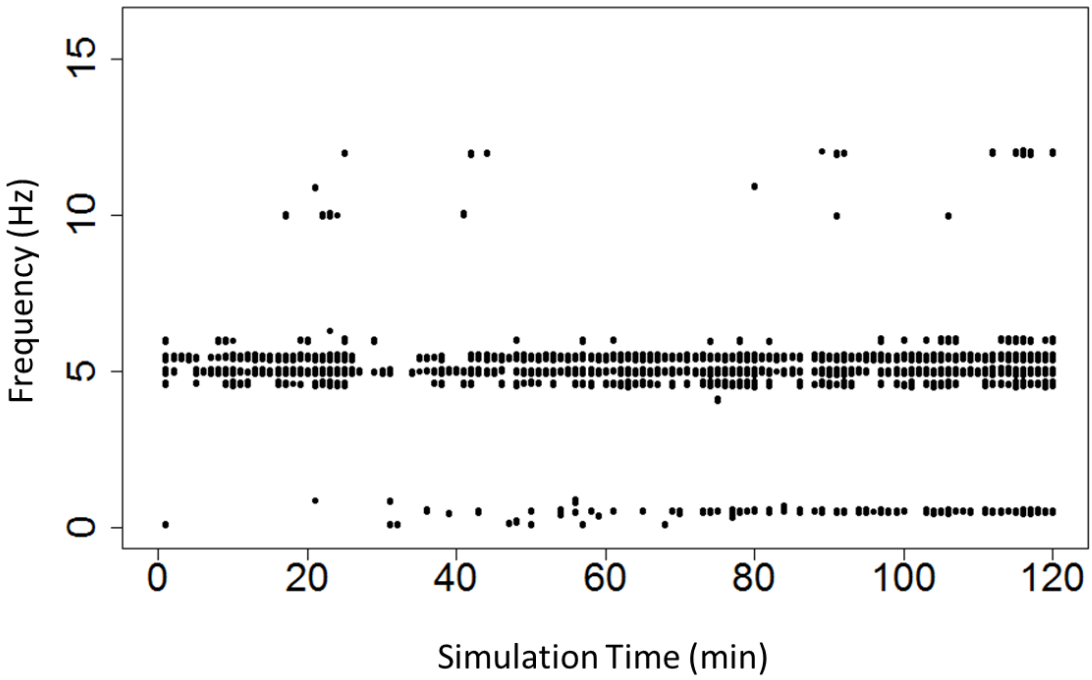

Figure 13: Detected forced oscillations in two hours of measurement data using the spectral-coherence method.

4.0 Conclusions

Forced oscillations are a growing concern for power system engineers. These oscillations are often associated with the malfunction or misoperation of power system equipment and can hinder the operation of the grid. Detecting forced oscillations is the first step in addressing the problem leading to the oscillation. In this report, multi-channel extensions to the previously developed periodogram and spectral-coherence methods of forced oscillation detection were developed and shown to improve upon their single channel counterparts.

The multi-channel methods described in this report both operate by comparing frequency domain test statistics to thresholds, but they differ significantly from each other in several other ways. A primary advantage of the periodogram method is that the relationship between the detection threshold and the probabilities of detection and false alarm can be expressed formulaically. The method's primary weakness is its dependence on estimates of the ambient noise spectra and the GMSC spectrum, which can be difficult to obtain reliably. The self-coherence method is relatively straightforward to implement, but a theoretical association between its threshold and probabilities of detection and false alarm does not exist. The periodogram method was shown to provide superior detection of small oscillations. However, because the spectral-coherence method must operate on smaller windows of data, it is able to detect large-amplitude forced oscillations faster in the online environment. With each method possessing strengths and weaknesses, the selection of a method should be based on the application. Many benefits, including verification, could be obtained by implementing the methods in parallel.

Future development work with the reported methods will focus on using their outputs to identify the sources of oscillations and exploring efficient implementations of the GMSC. Opportunities to implement the methods with large sets of archived PMU data and in the online environment will also be sought. Power system engineers have only recently recognized the prevalence of forced oscillations, providing an excellent opportunity to implement multi-channel forced oscillation detection methods to improve grid operation.

5.0 References

Follum, J. and Pierre, J.W., "Detection of Periodic Forced Oscillations in Power Systems," *Power Systems, IEEE Transactions on,* In Press.

Johnson, N.L., Kotz, S., and Balakrishnan, N., Continuous Univariate Distributions (Wiley Series in Probability and Statistics), Volume 2, Second Edition. Wiley-Interscience, 1995.

Kay, S.M., Fundamentals of Statistical Signal Processing, Volume 2: Detection Theory. Prentice Hall, 1998.

Ramirez, D., Via, J., and Santamaria, I., "A Generalization of the Magnitude Squared Coherence Spectrum for More than Two Signals: Definition, Properties, and Estimation," *Acoustics, Speech and Signal Processing, IEEE International Conference on (ICASSP),* pp. 3769-3772, March 31-April 4 2008.

Stoica, P. and Moses, R.L., Spectral Analysis of Signals, Pearson/Prentice Hall Upper Saddle River, N.J, 2005.

Trudnowski, D., Kosterev, D., and Undrill, J., "PDCI Damping Control Analysis for the Western North American Power System," *Power and Energy Society General Meeting (PES), 2013 IEEE*, 21-25 July 2013.

Zhou, N., "A Coherence Method for Detecting and Analyzing Oscillations," *Power and Energy Society General Meeting (PES), 2013 IEEE*, 21-25 July 2013.

Zhou, N. and Dagle, J., "Initial Results in Using a Self-Coherence Method for Detecting Sustained Oscillations," *Power Systems, IEEE Transactions on*, vol.30, no.1, pp.522,530, Jan. 2015.

Appendix A

Derivation of the Test Statistic for the Linear Model of a Sinusoid Embedded in Gaussian White Noise

The detector and test statistic proposed in this report were inspired by the detector for the simplified case of sinusoids with unknown parameters embedded in Gaussian white noise at several measurement locations. In this appendix, the theory for this simplified case is developed based on the detector for a deterministic signal with unknown parameters in complex white Gaussian noise described in Section 3.6.6 of [Kay, 1998]. The case considered here is a special case where the deterministic signal is a sinusoid and the noise is not complex. The resulting test and test statistic are closely related to those proposed for the detection of forced oscillations in this report.

For the m^{th} channel, the data model is

$$x_m[n] = w_m[n] + s_m[n]$$

where $w_m[n]$ is zero-mean white Gaussian noise and the signal model is

$$s_m[n] = A_m \cos(\omega_{FO} n + \zeta_m)$$

It is advantageous to write the signal model as a linear function of the unknown amplitude and phase. The unknown frequency will be addressed separately at the end of the derivation. Through trigonometry,

$$s_m[n] = [B_m \cos(\omega_{FO} n) - C_m \sin(\omega_{FO} n)]$$

where

$$A_m = \sqrt{B_m^2 + C_m^2}$$

$$\zeta_m = \tan^{-1}\left(\frac{C_m}{B_m}\right)$$

$$B_m = A_m \cos(\zeta_m)$$

$$C_m = A_m \sin(\zeta_m)$$

Letting $\tilde{\boldsymbol{s}}[n]$ denote the vector of signal models from the M channels at sample n, the collection of signal models for N samples is given by

$$s = \begin{bmatrix} s[0] \\ s[1] \\ \vdots \\ s[N-1] \end{bmatrix}$$

Using the previously described parameterization of $s_m[n]$, the full signal model can be written as

$$s = \underbrace{\begin{bmatrix} h_1[0] & h_2[0] & \cdots & h_{2M}[0] \\ h_1[1] & h_2[1] & \cdots & h_{2M}[1] \\ \vdots & \vdots & \ddots & \vdots \\ h_1[N-1] & h_2[N-1] & \cdots & h_{2M}[N-1] \end{bmatrix}}_{\tilde{H}} \theta$$

where each $h_i[n]$ is an M element vector and

$$\theta = [B_1 \quad C_1 \quad B_2 \quad C_2 \quad \cdots \quad B_M \quad C_M]^T$$

For odd i, all elements of $h_i[n]$ are zero except for element $\frac{i+1}{2}$, which is $\cos(\omega_{FO} \times n)$. For even i, all elements of $h_i[n]$ are zero except for element $\frac{i}{2}$, which is $-\sin(\omega_{FO} \times n)$. As shown in [Kay, 1998], a GLRT can be applied based on this linear model with the test statistic

$$T_w = \frac{\hat{\theta}_1^T H^T H \hat{\theta}_1}{\sigma^2} = \frac{\hat{s}^T x}{\sigma^2}$$

where

$$\hat{\theta}_1 = (H^T H)^{-1} H^T x$$

$$x = \begin{bmatrix} x[0] \\ x[1] \\ \vdots \\ x[N-1] \end{bmatrix}$$

$$\hat{s} = H \hat{\theta}_1$$

The subscript w denotes that this test statistic is derived for white Gaussian noise. Note that

$$H^T H = \begin{bmatrix} H_1 & 0 & \cdots & 0 \\ 0 & H_2 & \cdots & 0 \\ \vdots & \vdots & \ddots & \vdots \\ 0 & 0 & \cdots & H_M \end{bmatrix}$$

where

$$H_m = \begin{bmatrix} \sum_{n=0}^{N-1} \cos^2(\omega_{FO} \times n) & -\sum_{n=0}^{N-1} \cos(\omega_{FO} \times n) \times \sin(\omega_{FO} \times n) \\ -\sum_{n=0}^{N-1} \cos(\omega_{FO} \times n) \times \sin(\omega_{FO} \times n) & \sum_{n=0}^{N-1} \sin^2(\omega_{FO} \times n) \end{bmatrix} \approx \frac{N}{2} \times \boldsymbol{I}$$

Thus,

$$(H^T H)^{-1} \approx \frac{2}{N} \times I$$

Plugging this expression into the expression for $\hat{\theta}_1$ leads to

$$\hat{\theta}_1 \approx \frac{2}{N} \times I H^T \tilde{x} = \frac{2}{N} \sum_{n=0}^{N-1} \begin{bmatrix} x_1[n] \cos(\omega_{FO} \times n) \\ -x_1[n] \sin(\omega_{FO} \times n) \\ x_2[n] \cos(\omega_{FO} \times n) \\ -x_2[n] \sin(\omega_{FO} \times n) \\ \vdots \\ x_M[n] \cos(\omega_{FO} \times n) \\ -x_M[n] \sin(\omega_{FO} \times n) \end{bmatrix}$$

The test statistic then becomes

$$T_w = \frac{\hat{s}^T x}{\sigma^2} = \frac{\hat{\theta}_1^T \times H^T x}{\sigma^2} = \frac{\hat{\theta}_1^T \times \frac{N}{2} \hat{\theta}_1}{\sigma^2}$$

$$= \frac{1}{\sigma^2} \times \frac{4}{N^2} \times \frac{N}{2} \times \sum_{m=1}^{M} \left[\left(\sum_{n=0}^{N-1} x_m[n] \cos(\omega_{FO} \times n) \right)^2 + \left(-\sum_{n=0}^{N-1} x_M[n] \sin(\omega_{FO} \times n) \right)^2 \right]$$

$$= \frac{2}{N\sigma^2} \sum_{m=1}^{M} \left| \sum_{n=0}^{N-1} x_m[n] (\cos(\omega_{FO} \times n) - j \sin(\omega_{FO} \times n)) \right|^2$$

$$= \frac{2}{\sigma^2} \sum_{m=1}^{M} \frac{1}{N} \left| \sum_{n=0}^{N-1} x_m[n] e^{-j\omega_{FO} n} \right|^2$$

$$= \sum_{m=1}^{M} \frac{2\hat{\phi}_{x_m}(\omega_{FO})}{\sigma^2}$$

Thus, the test statistic is the sum of the periodograms for each sensor scaled by two divided by the variance.

Note that the test statistic is evaluated at the frequency of the forced oscillation, which is unknown. As suggested in Section 7.6.3 of [Kay, 1998], when the frequency of the sinusoids is unknown, the test statistic is calculated for a variety of frequencies. The detector decides that a sinusoid is present if the

peak value of the scaled sum of periodograms exceeds a threshold, and if so, the frequency location of that peak is the Maximum Likelihood Estimate (MLE) of the frequency. In this application though, forced oscillations often appear with harmonics, so the number of sinusoids is unknown. Thus, the statistic must be evaluated at a range of frequencies. Any frequency where the test statistic crosses the threshold serves as the frequency estimate for a detected forced oscillation. The test statistic is then written as

$$T_w(\omega_k) = \sum_{m=1}^{M} \frac{2\hat{\phi}_{x_m}(\omega_k)}{\sigma^2}$$

Here the frequency parameter has been discretized as

$$\omega_{\mathrm{k}} = \frac{2\pi k}{N^{(0)}}\,, \qquad 0 \le k \le \frac{N^{(0)}}{2}$$

where $N^{(0)}$ is the zero padded length of the periodogram.

Appendix B

Derivation of the Detection Threshold for Independent Channels

In this appendix, the test statistic's distribution and the associated P_{FA} are derived for the case where all channels are independent. The test statistic for the proposed detector is

$$T(\omega_k) = \sum_{m=1}^{M} \frac{2\hat{\phi}_{x_m}(\omega_k)}{\phi_{c_m}(\omega_k)}$$

To determine the P_{FA}, the case where the system is in ambient conditions, i.e., no forced oscillations are present, must be considered. For the remainder of this appendix, this case is assumed. From [Follum, 2015],

$$\frac{2\hat{\phi}_{x_m}(\omega_k)}{\phi_{c_m}(\omega_k)} \sim \chi_2^2 \tag{B1}$$

as $N \to \infty$ where χ_2^2 denotes a chi-squared random variable with two degrees of freedom. The sum of independent chi-squared random variables is distributed as a chi-squared random variable with degrees of freedom equal to the sum of the individual degrees of freedom [Johnson, 1995]. Thus,

$$T(\omega_k) \sim \chi_{2M}^2$$

Let Ω_B denote the length B set of frequency bins ω_k that are examined for forced oscillations. Then for the detection threshold $\gamma_\perp$,

$$\begin{aligned} P_{FA} &= P\big(\max\big(T(\omega_k)\big) > \gamma_\perp\big) \\ &= 1 - P\big(\max\big(T(\omega_k)\big) \le \gamma_\perp\big) \\ &= 1 - P\left(\bigcap_{\omega_k \in \Omega_B} [T(\omega_k) \le \gamma_\perp]\right) \end{aligned}$$

$$\leq B - \sum_{\omega_k \in \Omega_B} P(T(\omega_k) \leq \gamma_\perp)$$

$$= B - B \times F_{\chi^2_{2M}}(\gamma_\perp)$$

where the inequality is necessary because the frequency bins of the periodograms are not independent due to zero padding (see [Follum, 2015] for details) and $F_{\chi^2_d}(\cdot)$ denotes the CDF of the chi-squared random variable with d degrees of freedom. This equation can be rearranged to obtain an expression for the detection threshold for which the probability of false alarm will not exceed P_{FA}^{max} as

$$\gamma_\perp = F^{-1}_{\chi^2_{2\mathrm{M}}}\left(1 - \frac{P_{FA}^{max}}{B}\right)$$

where $F^{-1}_{\chi^2_d}(\cdot)$ denotes the inverse CDF.

Appendix C

Derivation of the Detection Threshold for Identical Channels

In this appendix, an expression relating the test statistic to P_{FA} is derived for the case where all channels are identical. When all channels are identical, the test statistic for the proposed detector can be written as

$$T(\omega_k) = \sum_{m=1}^{M} \frac{2\hat{\phi}_{x_m}(\omega_k)}{\phi_{c_m}(\omega_k)} = M \frac{2\hat{\phi}_{x_m}(\omega_k)}{\phi_{c_m}(\omega_k)}$$

To determine the P_{FA}, the case where the system is in ambient conditions, i.e., no forced oscillations are present, must be considered. For the remainder of this appendix, this case is assumed. From [Follum, 2015],

$$\frac{2\hat{\phi}_{x_m}(\omega_k)}{\phi_{c_m}(\omega_k)} \sim \chi_2^2 \tag{B1}$$

as $N \to \infty$ where χ_2^2 denotes a chi-squared random variable with two degrees of freedom. Let Ω_B denote the length B set of frequency bins ω_k that are examined for forced oscillations. Then for the detection threshold $\gamma_{\equiv}$,

$$\begin{aligned} P_{FA} &= P\big(\max\big(T(\omega_k)\big) > \gamma_{\equiv}\big) \\ &= 1 - P\big(\max\big(T(\omega_k)\big) \leq \gamma_{\equiv}\big) \\ &= 1 - P\left(\bigcap_{\omega_k \in \Omega_B} [T(\omega_k) \leq \gamma_{\equiv}]\right) \\ &\leq B - \sum_{\omega_k \in \Omega_B} P(T(\omega_k) \leq \gamma_{\equiv}) \end{aligned}$$

$$= B - B \times P\left(\frac{2\hat{\phi}_{x_m}(\omega_k)}{\phi_{c_m}(\omega_k)} \leq \frac{1}{M}\gamma_{\equiv}\right)$$

$$= B - B \times F_{\chi_2^2}\left(\frac{1}{M}\gamma_{\equiv}\right)$$

where the inequality is necessary because the frequency bins of the periodograms are not independent due to zero padding (see [Follum, 2015] for details) and $F_{\chi_d^2}(\cdot)$ denotes the CDF of the chi-squared random variable with d degrees of freedom. This equation can be rearranged to obtain an expression for the detection threshold for which the probability of false alarm will not exceed P_{FA}^{max} as

$$\gamma_{\equiv} = M \times F_{\chi_2^2}^{-1}\left(1 - \frac{P_{FA}^{max}}{B}\right)$$

where $F_{\chi_d^2}^{-1}(\cdot)$ denotes the inverse CDF.

Appendix D

Generalized Magnitude Squared Coherence

The Generalized Magnitude Squared Coherence (GMSC) is, as its name implies, a generalization of the Magnitude Squared Coherence (MSC). The MSC is a well-established, frequency-dependent measure of the linear relationship between two signals. It is described in [Stoica, 2005], as well as many other texts. The GMSC extends the MSC to more than two channels. For a complete description of the GMSC, see [Ramirez, 2008]. Here, a brief mathematical overview is provided.

The complex coherence spectrum is defined as

$$C_{x_i x_j}(\omega) = \frac{\phi_{x_i x_j}(\omega)}{\sqrt{\phi_{x_i}(\omega) \times \phi_{x_j}(\omega)}}, \qquad \forall\ i, j = 1, \dots, M$$

where M is the number of channels, $\phi_{x_i x_j}(\omega)$ is the cross-spectrum, and $\phi_{x_i}(\omega)$ is the PSD [Stoica, 2005]. The complex coherence spectra are arranged in a matrix such that

$$\Sigma_x(\omega) = \begin{bmatrix} 1 & C_{x_1 x_2}(\omega) & \vdots & C_{x_1 x_M}(\omega) \\ C_{x_2 x_1}(\omega) & 1 & \vdots & C_{x_2 x_M}(\omega) \\ \vdots & \vdots & \ddots & \vdots \\ C_{x_M x_1}(\omega) & C_{x_M x_2}(\omega) & \vdots & 1 \end{bmatrix}$$

Then the GMSC is defined as

$$G(\omega) = \frac{1}{(M-1)^2}\left(\lambda_{MAX}\left(\Sigma_x(\omega)\right) - 1\right)$$

where $\lambda_{MAX}\left(\Sigma_x(\omega)\right)$ denotes the largest eigenvalue of the matrix $\Sigma_x(\omega)$. As shown in [Ramirez, 2008], the GMSC is bounded between zero and one. To estimate the GMSC, the true cross-spectra and PSDs are replaced with estimates. Several methods of obtaining these estimates are described in [Stoica, 2005], including Welch's method averaging, which was utilized for the results presented in this report.

Distribution

No. of Copies

1 Philip Overholt
Department of Energy
1000 Independence Ave. SW
OE-40
Washington, DC 20585
(PDF)

1 Joseph Eto
1 Cyclotron Road
MS 90R4000
Berkeley, CA 94720
(PDF)

No. of Copies

4 **Local Distribution**
Pacific Northwest National Laboratory
Eric Andersen (PDF)
Jeff Dagle (PDF)
James Follum (PDF)
Francis Tuffner (PDF)

Pacific Northwest
NATIONAL LABORATORY

Proudly Operated by **Battelle** *Since 1965*

U.S. DEPARTMENT OF
ENERGY

902 Battelle Boulevard
P.O. Box 999
Richland, WA 99352
1-888-375-PNNL (7665)

www.pnnl.gov